

---

# NYUSIM User Manual

---

Version 1.5  
Copyright 2017  
New York University and NYU WIRELESS

April 5, 2017

# NYUSIM — User License

Copyright (c) 2017 New York University and NYU WIRELESS

Permission is hereby granted, free of charge, to any person obtaining a copy of this software and associated documentation files (the “Software”), to deal in the Software without restriction, including without limitation the rights to use, copy, modify, merge, publish, distribute, sublicense, and/or sell copies of the Software, and to permit persons to whom the Software is furnished to do so, subject to the following conditions:

The above copyright notice and this permission notice shall be included in all copies or substantial portions of the Software. Users shall cite NYU WIRELESS publications regarding this work.

THE SOFTWARE IS PROVIDED “AS IS”, WITHOUT WARRANTY OF ANY KIND, EXPRESS OR IMPLIED, INCLUDING BUT NOT LIMITED TO THE WARRANTIES OF MERCHANTABILITY, FITNESS FOR A PARTICULAR PURPOSE AND NONINFRINGEMENT. IN NO EVENT SHALL THE AUTHORS OR COPYRIGHT HOLDERS BE LIABLE FOR ANY CLAIM, DAMAGES OR OTHER LIABILITY, WHETHER IN AN ACTION OF CONTRACT, TORT OR OTHERWISE, ARISING FROM, OUT OF OR IN CONNECTION WITH THE SOFTWARE OR THE USE OR OTHER DEALINGS IN THE SOFTWARE.

# NYUSIM Overview

NYU WIRELESS conducted millimeter-wave (mmWave) measurements from 2012 through 2017, having acquired a total of over 1 Terabytes of data, at frequencies from 28 to 73 GHz in various outdoor environments in urban microcell (UMi), urban macrocell (UMa), and rural macrocell (RMa) environments. The measurements and analysis done in [1]–[9] led to this NYUSIM channel simulator.

NYUSIM provides an accurate rendering of actual channel impulse responses in both time and space, as well as realistic signal levels that were measured, and may be utilized to support realistic physical layer and link layer simulations such as those conducted in [10], [11]. The models and simulation approach in NYUSIM involves the research of more than a dozen graduate and undergraduate students, and as of early 2017, over 7,000 downloads of NYUSIM have been recorded. NYUSIM is applicable for a wide range of carrier frequencies from 500 MHz to 100 GHz, and RF bandwidths from 0 to 800 MHz.

It is worth noting that in the 3GPP TR 38.900 Release 14 channel model for frequencies above 6 GHz [12], the number of clusters is unrealistically large. For example, in the UMi street canyon scenario, the number of clusters in the LOS environment is as high as 12, and 19 in the NLOS environment, which is not supported by the real-world measurements at mmWave bands [1]–[4]. In contrast, in the SSCM implemented in NYUSIM [3], the number of time clusters ranges from 1 to 6, and the mean number of spatial lobes is about 2 and is upper-bounded by 5, which are obtained from field observations and are much smaller than those in the 3GPP channel model [12]. The impractical number of clusters in the 3GPP channel model is likely to result in a higher rank of mmWave channels, unrealistic eigenchannel distributions, and thereby inaccurate spectral efficiency prediction for 5G mmWave channels.

The current NYUSIM software package is Version 1.5 created on April 5th, 2017. Besides this user manual, five other files are provided and available for download from the website: <http://wireless.engineering.nyu.edu/5g-millimeter-wave-channel-modeling-software/>. The other five files are listed and explained as follows:

- NYUSIM — Channel Model Simulator Application: A standalone application that contains a graphical user interface (GUI) for NYU’s channel simulator, which will be detailed in the first two sections of this user manual. This application can run on computers with Windows 7 or higher and Mac operating systems (with or without MATLAB installed).
- Base Code: The MATLAB code used in the current version of NYUSIM to generate various channel parameters, which is created according to the millimeter-wave (mmWave) broadband statistical spatial channel model (SSCM) presented in [3]. The “Base Code” is applicable to arbitrary center carrier frequencies ranging from 500 MHz to 100 GHz,

arbitrary RF bandwidths from 0 to 800 MHz, and multi-antenna systems. Additionally, atmospheric attenuation effects, which includes the attenuation induced by dry air (containing oxygen), vapor, haze/fog, and rain, are also considered in the path loss model in the “Base Code” (more details can be found in Section 3 of this user manual).

- Time cluster - spatial lobe approach to cluster any measured or Ray traced data: The MATLAB code implementing the time cluster - spatial lobe (TCSL) algorithm used in the SSCM [3].
- User License: The user license for NYUSIM, which is also shown on the previous page of this user manual.
- Application Example Code: The example MATLAB code for possible applications that make use of NYUSIM.

## New Features in Version 1.5

Compared with NYUSIM Version 1.4 (v1.4), there are several major new features added to v1.5, which are detailed below.

The name of the output figure "Omni. PDP with Directional Antenna Gains" is changed to "Directional Power Delay Profile (PDP) with Strongest Power" to make it more accurate. Textual information on channel parameter values, such as frequency, environment, distance, root-mean-square (RMS) delay spread, received power, path loss, is added to the output figure "Directional PDP with Strongest Power", in which the path loss equals the transmit power subtracted by the transmitter (TX) and receiver (RX) antenna gains and the received power.

Besides the existing output figures, one additional output figure entitled "PathLossPlot" is added if the user performs  $N$  ( $N \geq 1$ ) continuous simulation runs with the same input parameters but with varying distances. The figure "PathLossPlot" illustrates a scatter plot of omnidirectional path loss and directional path loss values for over the entire distance range generated from the  $N$  continuous simulation runs, along with the fitted path loss exponent (PLE) and shadow fading standard deviation. Detailed information about the figure "PathLossPlot" is provided in Section 2.2.1 of this user manual.

Four additional output data files, namely, "OmniPDPInfo.txt", "DirPDPInfo.txt", "OmniPDPInfo.mat", and "DirPDPInfo.mat", are added after  $N$  continuous simulation runs with the same input parameters are performed by the user. "Omni" denotes omnidirectional, while "Dir" stands for directional. Detailed descriptions about these four files were added in Section 2.2.2 of this user manual. Furthermore, the output files "BasicParameters.txt" and "BasicParameters.mat" are generated only once for all  $N$  continuous simulation runs with the same input parameters, instead of being generated for each individual simulation run, since the parameters contained in these two files remain the same for  $N$  continuous simulation runs. Two parameter values in each of the two output files "BasicParameters.txt" and "BasicParameters.mat", i.e., omnidirectional received power and omnidirectional path loss, are removed since they are now included in the new output files "OmniPDPInfo.txt" and "OmniPDPInfo.mat". Therefore, if a user perform  $N$  continuous simulation runs and select both .txt and .mat formats for the output data files, the following files will be generated:

- $N$  AOD power spectrum figures (AOD\_Run $n$ .png)
- $N$  AOA power spectrum figures (AOA\_Run $n$ .png)
- $N$  omnidirectional PDP figures (OmniPDP\_Run $n$ .png)
- $N$  directional PDP figures (DirPDP\_Run $n$ .png)
- $N$  small-scale PDP figures (SmallScalePDP\_Run $n$ .png)
- One omnidirectional and directional path loss scatter plot (PathLossPlot.png)

- $N$  sets of AODLobePowerSpectrum text files
- $N$  sets of AOALobePowerSpectrum text files
- $N$  OmniPDP text files
- $N$  DirectionalPDP text files
- $N$  SmallScalePDP text files
- One BasicParameters text file
- One OmniPDPInfo text file
- One DirPDPInfo text file
- $N$  AODLobePowerSpectrum MAT files
- $N$  AOALobePowerSpectrum MAT files
- $N$  OmniPDP MAT files
- $N$  DirectionalPDP MAT files
- $N$  SmallScalePDP MAT files
- One BasicParameters MAT file
- One OmniPDPInfo MAT file
- One DirPDPInfo MAT file

Detailed explanation on how the directional PDP with strongest power is generated is added in Section 2.2.1 of this user manual. Examples of the six output figures from NYUSIM are added in Section 2.2.1 of this user manual. The MATLAB code "getChannelMatrix" and the associated explanation in the NYUSIM application code package are updated according to the new output data files. Moreover, a new chapter (Chapter 4) is created to present a variety of applications of NYUSIM. The original application section in Chapter 2 is also moved to Chapter 4. Finally, a new version of the NYUSIM software is created for the Mac operating system, with all of the above updates implemented. Installation instructions are provided in Section 1 of this user manual.

## *Acknowledgements*

We would like to thank Mr. Michael G. Cotton at the National Telecommunications & Information Administration (NTIA) for providing the reference and code on atmospheric attenuation characteristics at frequencies below 1000 GHz, which have been used in the NYUSIM channel simulator and this user manual.

This work is also supported by NYU WIRELESS Industrial Affiliates and National Science Foundation (NSF) (Award Number: 1555332, 1302336, and 1320472).

# Revision History

## 1. Ver 1.5: April 5th, 2017

- (a) A more detailed overview about the mmWave measurements on which NYUSIM has been built, the related publications, and key differences/advantages of the NYUSIM channel model as compared to the 3rd Generation Partnership Project (3GPP) TR 38.900 Release 14 channel model are added in NYUSIM Overview on Page ii of this user manual.
- (b) The name of the output figure "Omni. PDP with Directional Antenna Gains" is changed to "Directional Power Delay Profile (PDP) with Strongest Power" to make it more accurate. Textual information on channel parameter values, such as frequency, environment, distance, root-mean-square (RMS) delay spread, received power, path loss, is added to the output figure "Directional PDP with Strongest Power", in which the path loss equals the transmit power subtracted by the transmitter (TX) and receiver (RX) antenna gains and the received power.
- (c) One additional output figure entitled "PathLossPlot" is added if the user performs  $N$  ( $N \geq 1$ ) continuous simulation runs with the same input parameters but with varying distances. The figure "PathLossPlot" illustrates a scatter plot of omnidirectional path loss and directional path loss values for over the entire distance range generated from the  $N$  ( $N \geq 1$ ) continuous simulation runs, along with the fitted path loss exponent (PLE) and shadow fading standard deviation. Detailed information about the figure "PathLossPlot" is provided in Section 2.2.1 of this user manual.
- (d) Four additional output data files, namely, "OmniPDPInfo.txt", "DirPDPInfo.txt", "OmniPDPInfo.mat", and "DirPDPInfo.mat", are added after  $N$  ( $N \geq 1$ ) continuous simulation runs with the same input parameters are performed by the user. "Omni" denotes omnidirectional, while "Dir" stands for directional. Detailed descriptions about these four files were added in Section 2.2.2 of this user manual.
- (e) The output files "BasicParameters.txt" and "BasicParameters.mat" are generated only once for all  $N$  ( $N \geq 1$ ) continuous simulation runs with the same input parameters, instead of being generated for each individual simulation run, since the parameters contained in these two files remain the same for  $N$  ( $N \geq 1$ ) continuous simulation runs.
- (f) Two parameter values in each of the two output files "BasicParameters.txt" and "BasicParameters.mat", i.e., omnidirectional received power and omnidirectional path loss, are removed since they are now included in the new output files "OmniPDPInfo.txt" and "OmniPDPInfo.mat".
- (g) Detailed explanation on how the directional PDP with strongest power is generated is added in Section 2.2.1 of this user manual.

- (h) Examples of the six output figures from NYUSIM are added in Section 2.2.1 of this user manual.
- (i) Error warnings are added for the cases where the input antenna HPBW by the user exceeds the pre-defined range on the GUI. Explanations are detailed in Section 2.1.5 of this user manual.
- (j) Figs. 3.1 and 3.2 in Section 3.1 are modified where the humidity is changed from 98% to 80%, and temperature is changed from  $-20^{\circ}\text{C}$  to  $20^{\circ}\text{C}$ , to reflect more realistic atmospheric conditions.
- (k) A new chapter (Chapter 4) is created to present a variety of applications of NYUSIM. The original application section in Chapter 2 is also moved to Chapter 4.
- (l) The MATLAB code "getChannelMatrix" and the associated explanation in the NYUSIM application code package are updated according to the new output data files.
- (m) The root folder for users to select from to save output files is changed from the C drive to the folder "Users".
- (n) A new version of the NYUSIM software is created for the Mac operating system, with all of the above updates implemented. Installation instructions are provided in Section 1.

## 2. Ver 1.4: October 31st, 2016

- (a) More operation steps were added on the top part of the simulator GUI to better instruct users.
- (b) Detailed explanations of the half-power beamwidth (HPBW) and gain of the antenna array, and examples of how to create an antenna pattern given the HPBW and gain, were added in Section 2.1.1 of this user manual.
- (c) The .mat format of the output data files was provided in the simulator, in addition to the existing .txt files. Descriptions of the newly added files were provided in Section 2.2.2 of this user manual. A new option was added on the GUI that allows users to select the output file type (text file, MAT file, or both).
- (d) A new set of output data file named "BasicParameters" was added with both .txt and .mat formats available, which contains all the input parameter values as shown on the GUI when running the simulation and some relevant output parameters, as detailed in Section 2.2.2.
- (e) An example of the applications of the output data files was demonstrated in Section 2.2.3, namely, calculating the condition number and rank of multiple-input multiple-output (MIMO) orthogonal frequency division multiplexing (OFDM) channel matrices, and the corresponding MATLAB script was provided in the package named "Application Example Code" available on the NYUSIM downloading website.

## 3. Ver 1.3: August 19th, 2016

- (a) Descriptions of the numbers of matrix columns and rows in the output .txt files containing the complex channel coefficients ( $H$ ),

phases (HPhases), and powers (HPowers) were corrected in Section 2.2.2 of this user manual.

- (b) The rural macrocell (RMA) path loss parameters in the close-in reference distance (CI) path loss model have been slightly changed in the simulator and Section 3.1 of this user manual, based on the new mmWave rural path loss study in [8].
- (c) The new frequency range of the simulator has been tested and is usable from 500 MHz to 100 GHz.

#### 4. Ver 1.2: August 2nd, 2016

- (a) Four new input parameters, i.e., Polarization, Foliage Loss, Distance Within Foliage, and Foliage Attenuation, were added to the input parameters on the NYUSIM GUI, the corresponding code was added to the base code, and the corresponding descriptions of the four new input parameters were added in Section 2 of the user manual.
- (b) The NYU CI RMA path loss model was added to the simulator and user manual, and the option “RMA” was added to the “Scenario” parameter on the GUI.
- (c) More background regarding the creation and application of NYUSIM was added to the section *NYUSIM Overview*, and two related citations were added to the reference list.
- (d) A 32-bit version of NYUSIM was generated, in addition to the existing 64-bit version.

#### 5. Ver 1.1: July 16th, 2016

- (a) Four new input parameters, i.e., Barometric Pressure, Humidity, Temperature, and Rain Rate, were added to the input parameters on the NYUSIM GUI, the corresponding code was added to the base code, and the corresponding descriptions of the four new input parameters were added in Section 2 of the user manual.

# Contents

|  |            |
|--|------------|
| <b>NYUSIM — User License</b>   | <b>i</b>   |
| <b>NYUSIM Overview</b>   | <b>ii</b>  |
| <b>New Features in Version 1.5</b>   | <b>iv</b>  |
| <b>Acknowledgements</b>  | <b>vi</b>  |
| <b>Revision History</b>  | <b>vii</b> |
| <b>1 Installation of Software Package</b>  | <b>1</b>   |
| 1.1 System Requirements . . . . .  | 1          |
| 1.1.1 Operating System . . . . .   | 1          |
| 1.2 Installation . . . . .   | 1          |
| 1.2.1 Windows Operating System . . . . .   | 1          |
| 1.2.2 Mac OS X . . . . .   | 2          |
| <b>2 Basics</b>  | <b>3</b>   |
| 2.1 Graphical User Interface and Simulator Basics . . . . .                            | 3          |
| 2.1.1 Input Parameters . . . . .   | 3          |
| 2.1.2 Output Folder Selection . . . . .  | 8          |
| 2.1.3 Output File Type Selection . . . . .   | 9          |
| 2.1.4 Operation of the GUI . . . . .   | 9          |
| 2.2 Output Files . . . . .   | 10         |
| 2.2.1 Output Figures . . . . .   | 10         |
| 2.2.2 Output Data Files . . . . .  | 12         |
| <b>3 Channel Model Supported by NYUSIM</b>   | <b>18</b>  |
| 3.1 Path Loss Model . . . . .  | 18         |
| 3.2 Wideband Temporal/Spatial Clustering Algorithm . . . . .                           | 20         |
| <b>4 Applications of NYUSIM</b>  | <b>23</b>  |
| 4.1 MIMO Channel Condition Number . . . . .  | 23         |
| 4.2 Spectral Efficiency Comparison Between 3GPP and NYUSIM<br>Channel Models . . . . . | 27         |
| <b>Bibliography</b>  | <b>29</b>  |

## List of Figures

|     |   |    |
|-----|---|----|
| 2.1 | GUI of NYUSIM. . . . .  | 4  |
| 2.2 | Example of a 3D AOD power spectrum generated from NYUSIM. . . . .   | 12 |
| 2.3 | Example of a 3D AOA power spectrum generated from NYUSIM. . . . .   | 13 |
| 2.4 | Example of an omnidirectional PDP generated from NYUSIM. . . . .  | 13 |
| 2.5 | Example of a directional PDP with the strongest received power generated from NYUSIM. "Ant." denotes antenna. . . . .   | 14 |
| 2.6 | Example of the PDPs over different receive antenna elements generated from NYUSIM. . . . .  | 14 |
| 2.7 | Example of a scatter plot showing the omnidirectional and directional path loss values generated from NYUSIM with 100 simulation runs for the 28 GHz UMi LOS scenario. $n$ denotes the pass loss exponent (PLE), $\sigma$ is the shadow fading standard deviation, "omni" denotes omnidirectional, "dir" represents directional, "dir-best" means the direction with the strongest received power, "Ant." denotes antenna, "AZ" and "EL" stand for azimuth and elevation, respectively. . . . . | 15 |
| 3.1 | Propagation attenuation due to dry air, vapor, haze, and rain at mmWave frequencies, with a barometric pressure of 1013.25 mbar, a relative humidity of 80%, a temperature of 20°C, and a rain rate of 5 mm/hr [13]. . . . .  | 19 |
| 3.2 | Collective attenuation effects of dry air, vapor, haze, and rain at mmWave frequencies, with a barometric pressure of 1013.25 mbar, a relative humidity of 80%, a temperature of 20°C, and a rain rate of 5 mm/hr [13]. . . . .   | 19 |
| 3.3 | Example of an omnidirectional PDP with four multipath taps [3]. . . . .   | 21 |
| 3.4 | Example of an AOA power spectrum with four multipath taps [3]. . . . .  | 22 |
| 4.1 | Empirical CDF of the condition number of channel matrices for OFDM sub-carriers with different transmit and receive antenna elements $N_t$ and $N_r$ for MIMO-OFDM channels in one simulation run. . . . .  | 26 |
| 4.2 | Empirical CDF of the rank of channel matrices for OFDM sub-carriers with different transmit and receive antenna elements $N_t$ and $N_r$ for MIMO-OFDM channels in one simulation run. . . . .  | 26 |
| 4.3 | Spectral efficiency achieved by hybrid beamforming for a $256 \times 16$ system at 28 GHz with rectangular antenna arrays at the transmitter and receiver with four RF chains. . . . .  | 28 |

# 1. Installation of Software Package

## 1.1 System Requirements

### 1.1.1 Operating System

Minimum requirement: Windows 7 (or higher), or Macintosh operating systems (Mac OS X)

The Windows 32 bit version of NYUSIM runs on Windows 32 bit operating systems only, the Windows 64 bit version of NYUSIM runs on Windows 64 bit operating systems only, and the Mac version of NYUSIM runs on Mac OS X only.

## 1.2 Installation

The required program files of the NYUSIM software suite are provided by NYU WIRELESS via Internet download at <http://wireless.engineering.nyu.edu/5g-millimeter-wave-channel-modeling-software/>.

### 1.2.1 Windows Operating System

The Windows version of NYUSIM is delivered as an installer package for Windows operating systems. All components required to run the applications are automatically installed after double clicking on the setup executable, and following the step-by-step instructions therein. Below is an extra step to take before running the NYUSIM application:

Verify the MATLAB Runtime is installed and ensure you have installed version 9.1 (R2016b). If the MATLAB Runtime is not installed, do the following: (1) Enter "»mcrinstaller" at MATLAB prompt. The MCRINSTALLER command displays the location of the MATLAB Runtime installer. (2) Run the MATLAB Runtime installer. Alternatively, download the Windows 64-bit (or 32-bit) version of the MATLAB Runtime for R2016b from the MathWorks Web site by navigating to

<http://www.mathworks.com/products/compiler/mcr/index.html>.

For more information about the MATLAB Runtime and the MATLAB Runtime installer, see Package and Distribute in the MATLAB Compiler documentation in the MathWorks Documentation Center.

### 1.2.2 Mac OS X

The Mac version of NYUSIM is delivered as an installer package for Mac OS X. All components required to run the applications are automatically installed after double clicking on the setup executable, and following the step-by-step instructions therein. Below are some extra steps to take before running the NYUSIM application.

#### 1. Prerequisites for Deployment

Verify the MATLAB Runtime is installed and ensure you have installed version 9.1 (R2016b). If the MATLAB Runtime is not installed, do the following: (1) Enter "»mcrinstaller" at MATLAB prompt. The MCRINSTALLER command displays the location of the MATLAB Runtime installer. (2) Run the MATLAB Runtime installer. Alternatively, download the Macintosh version of the MATLAB Runtime for R2016b from the MathWorks Web site by navigating to

<http://www.mathworks.com/products/compiler/mcr/index.html>.

For more information about the MATLAB Runtime and the MATLAB Runtime installer, see Package and Distribute in the MATLAB Compiler documentation in the MathWorks Documentation Center.

#### 2. Files to Deploy and Package

Run NYUSIM\_v1\_5\_Mac.sh (shell script for temporarily setting environment variables and executing the application). To run the shell script, type `./run_NYUSIM_v1_5_Mac.sh <mcr_directory> <argument_list>` at Linux or Mac command prompt. `<mcr_directory>` is the directory where version 9.1 of the MATLAB Runtime is installed or the directory where MATLAB is installed on the machine. `<argument_list>` is all the arguments you want to pass to your application. For example, if you have version 9.1 of the MATLAB Runtime installed in `/mathworks/home/application/v91`, run the shell script as:

```
./run_NYUSIM_v1_5_Mac.sh /mathworks/home/application/v91.
```

If you have MATLAB installed in `/mathworks/devel/application/matlab`, run the shell script as:

```
./run_NYUSIM_v1_5_Mac.sh /mathworks/devel/application/matlab.
```

For additional support, please contact [nyusim@nyuwireless.com](mailto:nyusim@nyuwireless.com).

## 2. Basics

### 2.1 Graphical User Interface and Simulator Basics

The following screenshot (Fig. 2.1) shows the graphical user interface (GUI) of NYUSIM. The simulator performs Monte Carlo simulations, generating certain numbers of samples of channel impulse responses (CIRs) at specific T-R separation distances, where the number of samples and the range of T-R separation distances are to be specified by users, as explained in the following subsection. It takes about 22 minutes to generate and save 100 CIRs and all the output files (five .png files, seven sets of .txt files and seven .mat files for each CIR simulation run as detailed in Section 2.2) on a PC server with two processors (2.40 GHz and 2.39 GHz) and 96.0 GB RAM.

#### 2.1.1 Input Parameters

There are 28 input parameters to the channel simulator, which are grouped into two main categories: *Channel Parameters* and *Antenna Properties*, as shown on the GUI in Fig. 2.1. The panel *Channel Parameters* contains 16 fundamental input parameters about the propagation channel, as listed and explained below:

1. Frequency (GHz): an editable parameter denoting the carrier frequency in GHz. The default value is 28 (GHz), and it can be varied from 0.5 to 100 (GHz) with at most one decimal point.
2. RF Bandwidth (MHz): an editable parameter denoting the RF bandwidth of the transmitted signal in MHz. The default value is 800 MHz, and it can be varied from 0 to 800 MHz. As the simulator was developed from real-world measurements obtained with an RF bandwidth of 800 MHz, it can only scale down from 800 MHz.
3. Scenario: a selectable parameter denoting the scenario. Three options, "UMi", "UMa", and "RMa", are applicable. The channel parameters for the UMi scenario are also used for the UMa and RMa scenarios in this simulator, except that the RMa scenario has its own path loss model parameters. The default option is "UMi".

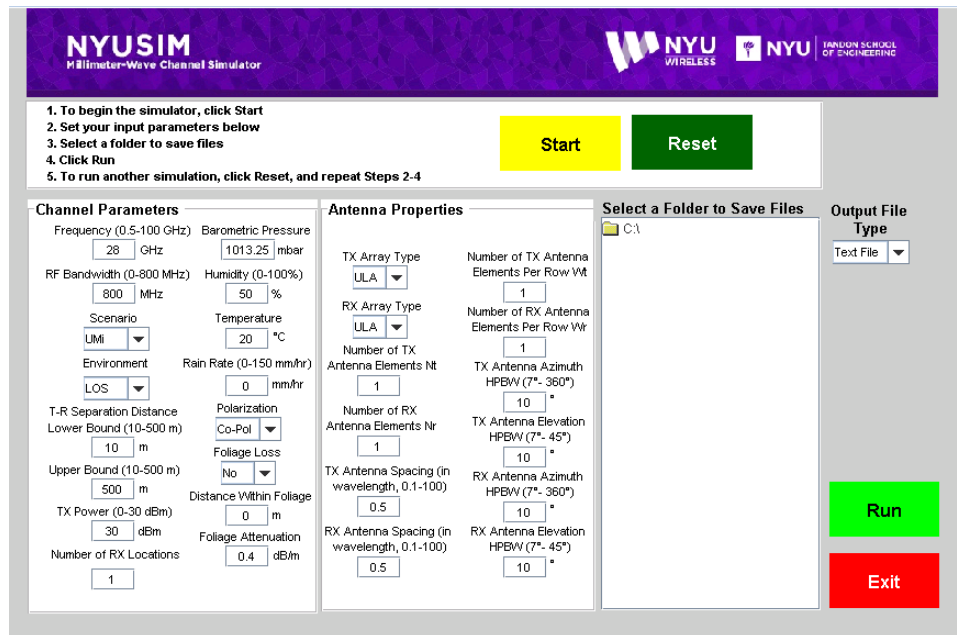


FIGURE 2.1: GUI of NYUSIM.

4. Environment: a selectable parameter denoting the environment, either line-of-sight (LOS) or non-line-of-sight (NLOS). The default setting is LOS.
5. Lower Bound of T-R Separation Distance (m): an editable parameter denoting the smallest distance between the transmitter (TX) and receiver (RX) in meters with at most one decimal place. The default value is 10 m, and it can be varied from 10 m to 500 m but no more than the upper bound of the T-R separation distance.
6. Upper Bound of T-R Separation Distance (m): an editable parameter denoting the largest distance between the TX and RX in meters with at most one decimal place. The default value is 500 m, and it can be varied from 10 m to 500 m but no less than the lower bound of the T-R separation distance.
7. TX Power (dBm): an editable parameter denoting the transmit power in dBm. The default value is 30 (dBm), and can be set to any value ranging from 0 to 30 (dBm).
8. Number of RX Locations: an editable parameter denoting the number of RX locations. It can be any positive integer number. The default value is 1, and can be set to any integer from 1 to 10,000.

9. Barometric Pressure: an editable parameter denoting the barometric pressure in mbar used in evaluating propagation path loss induced by dry air. The default and typical value is 1013.25 mbar (millibar) (i.e., nominal for sea level), and may range from  $10^{-5}$  to 1013.25 (mbar) [13].
10. Humidity: an editable parameter denoting the relative humidity in percentage used in evaluating propagation path loss induced by vapor. The default value is 50 (%), and can be set to any number between 0 and 100 (%).
11. Temperature: an editable parameter denoting the temperature in degrees Celsius used in evaluating propagation path loss induced by haze/fog. The default and typical value is 20 ( $^{\circ}\text{C}$ ), and may range from -100 to 50 ( $^{\circ}\text{C}$ ) [13].
12. Rain Rate: an editable parameter denoting the rain rate in mm/hr used in evaluating propagation path loss induced by rain. The default value is 0 (mm/hr), and the typical range is 0 to 150 (mm/hr) [1].
13. Polarization: a selectable parameter denoting the polarization relation between the TX and RX antennas or antenna arrays. The default setting is Co-Pol (co-polarization), and can be changed to X-Pol (cross-polarization). The cross polarization discrimination (XPD) can vary from 5 dB to 27 dB [14]–[16], depending on the frequency and environment. In this simulator, for Co-Pol, no extra loss will be added to the path loss, while an extra 25 dB loss will be added to the path loss for X-Pol due to polarization mismatch based on the measurement results in [16]. For more detailed background, please refer to [16].
14. Foliage Loss: a selectable parameter indicating whether or not foliage loss will be considered in the simulation. The default setting is No (which implies foliage loss will not be considered), and can be changed to Yes (which means foliage loss will be considered).
15. Distance Within Foliage: an editable parameter representing the distance in meters that the transmitted signal travels within foliage. The default value is 0, and can be set to any non-negative number no larger than the lower bound of the T-R separation distance.
16. Foliage Attenuation: an editable parameter denoting the propagation loss induced by foliage in dB/m. The default value is 0.4 (dB/m) based on the measurement results in [16], and can be set to any value between 0 and 10 (dB/m). For more detailed background, please refer to [16].

The panel *Antenna Properties* contains 12 input parameters related to the TX and RX antenna arrays, as listed and explained below:

1. TX Array Type: a selectable parameter denoting the TX antenna array type. The default setting is ULA (uniform linear array), and can be changed to URA (uniform rectangular array).
2. RX Array Type: a selectable parameter denoting the RX antenna array type. The default setting is ULA, and can be changed to URA.
3. Number of TX Antenna Elements  $N_t$ : an editable parameter denoting the total number of TX antenna elements in the array. The default value is 1, and can be set to any integer from 1 to 128.
4. Number of RX Antenna Elements  $N_r$ : an editable parameter denoting the total number of RX antenna elements in the array. The default value is 1, and can be set to any integer from 1 to 64.
5. TX Antenna Spacing (in wavelength): an editable parameter denoting the spacing between adjacent TX antennas in the array in terms of the carrier wavelength. The default value is 0.5, and can be set to any positive number with up to one decimal place from 0.1 to 100.
6. RX Antenna Spacing (in wavelength): an editable parameter denoting the spacing between adjacent RX antennas in the array in terms of the carrier wavelength. The default value is 0.5, and can be set to any positive number with up to one decimal place from 0.1 to 100.
7. Number of TX Antenna Elements Per Row  $W_t$ : an editable parameter denoting the number of TX antennas in one dimension when the TX Array Type is ULA or URA, which should divide the number of TX antenna elements. The default value is 1.
8. Number of RX Antenna Elements Per Row  $W_r$ : an editable parameter denoting the number of RX antennas in one dimension when the RX Array Type is ULA or URA, which should divide the number of RX antenna elements. The default value is 1.
9. TX Antenna Azimuth HPBW (degrees): an editable parameter denoting the azimuth half-power-beamwidth (HPBW) of the TX antenna (array) in degrees. The default value is  $10^\circ$ , and can be set to any value from  $7^\circ$  to  $360^\circ$  (since the smallest azimuth HPBW of the antennas used in the measurements for the simulator was  $7^\circ$ ).

10. TX Antenna Elevation HPBW (degrees): an editable parameter denoting the elevation HPBW of the TX antenna (array) in degrees. The default value is  $10^\circ$ , and can be set to any value from  $7^\circ$  to  $45^\circ$  (since the smallest elevation HPBW of the antennas used in the measurements for the simulator was  $7^\circ$ ).
11. RX Antenna Azimuth HPBW (degrees): an editable parameter denoting the azimuth HPBW of the RX antenna (array) in degrees. The default value is  $10^\circ$ , and can be set to any value from  $7^\circ$  to  $360^\circ$ .
12. RX Antenna Elevation HPBW (degrees): an editable parameter denoting the elevation HPBW of the RX antenna (array) in degrees. The default value is  $10^\circ$ , and can be set to any value from  $7^\circ$  to  $45^\circ$ .

It is worth noting that the HPBW in the input parameters is for the entire antenna array, instead of for each antenna element, when the number of antenna elements is more than one at the TX and/or RX. Conventionally, the HPBW of an antenna array is a function of the number of antenna elements and the antenna spacing, but in this simulator these three parameters (i.e., the HPBW, number of antenna elements, and antenna spacing) can be independently specified by the user, since there may be a wide range of beamforming approaches (e.g., digital, analog, hybrid), in all of which different individual antenna element types (e.g., patch antennas, vertical antennas, horns) may be used. To make the simulator as general as possible, we specify the number of individual antenna elements (without specifying the gain or combining losses thereof) and the total array HPBW. Note that the antenna pattern and implementation details are only very loosely defined to specify the gain in the particular pointing (maximum gain) direction.

Since some antenna elements may have more gain or loss depending on the specific array type (e.g., ULA); that is, someone may choose to fabricate their individual array with more individual antenna element gain than another person will, and losses vary with fabrication process (e.g., on chip antenna elements have more loss when a lens is not used than if a lens is used). Instead of dealing with the myriad antenna fab and connection details needed to make an array — there are numerous variables — we simply allow the total HPBW and the number of elements to be specified, without specifying the individual antenna element gain. For example, assuming there are four elements in an antenna array, where each element has 6 dB gain because they are patch or Yagi/directional or horn antennas for each element, then this array can have the same overall HPBW as a 16 element array with unity gain dipole or vertical elements.

Without specifying the specific antenna elements and their interconnected characteristics, only the HPBW is specified while the beam pattern is left undefined. Consequently, one has the freedom to implement an antenna pattern of their choice for system simulations, which may include interference from signals outside of the main gain direction. Here are some heuristic approaches of constructing one's own antenna pattern based on

the specified HPBW, where the antenna gains in the following equations are all relative to an isotropic antenna.

- The antenna pattern employed in [3] has the following form:

$$G(\theta, \phi) = \max(G_0 e^{-\alpha\theta^2 - \beta\phi^2}, \frac{G_0}{100}) \quad (2.1)$$

$$\alpha = \frac{4\ln(2)}{\theta_{3dB}^2}, \beta = \frac{4\ln(2)}{\phi_{3dB}^2}, G_0 = \frac{41253\eta}{\theta_{3dB}\phi_{3dB}}$$

where  $(\theta, \phi)$  denote the azimuth and elevation angle offsets from the boresight direction in degrees,  $G_0$  is the maximum directive gain (boresight gain) in linear units,  $(\theta_{3dB}, \phi_{3dB})$  represent the azimuth and elevation HPBWs in degrees,  $(\alpha, \beta)$  are parameters that depend on the HPBW values, and  $\eta = 0.7$  is a typical average antenna efficiency.

- The antenna pattern used in [6] has the expression below:

$$f(\phi, \theta) = G \left[ \text{sinc}^2(a \cdot \sin(\phi)) \cos^2(\phi) \right] \cdot \left[ \text{sinc}^2(b \cdot \sin(\theta)) \cos^2(\theta) \right] \quad (2.2)$$

where  $\phi$  and  $\theta$  represent the azimuth and elevation angles with respect to the antenna boresight, respectively,  $f(\phi, \theta)$  denotes the radiation power density at the azimuth angle  $\phi$  and elevation angle  $\theta$ ,  $G$  is the antenna boresight gain, and  $a$  and  $b$  are functions of the azimuth (AZ) and elevation (EL) HPBWs of the horn antenna, respectively, i.e.,

$$\text{sinc}^2\left(a \cdot \sin\left(\frac{\text{HPBW}_{AZ}}{2}\right)\right) \cos^2\left(\frac{\text{HPBW}_{AZ}}{2}\right) = \frac{1}{2} \quad (2.3)$$

$$\text{sinc}^2\left(b \cdot \sin\left(\frac{\text{HPBW}_{EL}}{2}\right)\right) \cos^2\left(\frac{\text{HPBW}_{EL}}{2}\right) = \frac{1}{2} \quad (2.4)$$

- The radiation pattern of a sectored cell site antenna was employed in [17], where the azimuthal radiation pattern is modeled as a cardioid given by [17]

$$r(\theta) = \alpha \left[ 1 + \sin\left(\theta + \frac{\pi}{2}\right) \right] \quad (2.5)$$

where  $r$  is the gain of the antenna at azimuth angle  $\theta$  from its maximum lobe and is a scaling factor. The elevation radiation pattern is an ellipse with the base station at a focus point [17]:

$$\frac{x^2}{a^2} + \frac{y^2}{b^2} = 1 \quad (2.6)$$

- A sectored antenna pattern model was introduced in [18], where constant directivity gains are assumed for the main lobe and the side lobe.

## 2.1.2 Output Folder Selection

To the right of the above two category panels (*channel parameters* and *antenna properties*) on the GUI, there is an option named "Select a Folder to

Save Files”. This option allows users to select a folder to save the output files (e.g., figures, data files) from the simulator. The default path is the disk that contains the current running folder. Users can select a folder inside the default path by clicking on the desired paths/folders.

### 2.1.3 Output File Type Selection

To the right of the folder selection option on the GUI, there is an option named “Output File Type”. This option allows users to select a file type for the output data files from the simulator. The default type is *Text File*, and can be switched to *MAT File*, and *Both Text and MAT File*.

### 2.1.4 Operation of the GUI

Five basic steps, as shown on the top left panel on the GUI, need to be executed to run the channel simulator:

1. To begin (reset) the simulator, click Start (Reset)
2. Set your input parameters below
3. Select a folder to save files
4. Click Run
5. To run another simulation, click Reset, and repeat Steps 2-4

The meanings of these steps are detailed as follows.

When opening the GUI for the first time, users shall click on the yellow button “Start” to initiate the simulator and enable the input of the GUI. Next, users can set and/or select the 28 input parameters according to their own needs; the simulator will execute the default values for each parameter if there is no input from the user. Then, users shall select a folder to save all the output files by clicking on the desired paths/folders under the option “Select a Folder to Save Files”. Finally, users shall click on the light green button “Run” to run the simulations.

While the simulator is running, a progress bar will pop up at the bottom left of the GUI, which informs users of the progress of the simulations. After the simulation is complete, the progress bar will disappear automatically, and the five figures generated from the first simulation run will pop up on the screen.

To initiate another set of simulation runs (e.g., with different input parameter values), users shall click on the dark green button “Reset”, after which all the input parameters from the previous simulation run will be set as the default input values.

The simulator can be closed at any time by clicking the red button “Exit” on the bottom right of the GUI.

If the input number of TX antenna elements per row  $W_t$  is larger than the input number of TX antenna elements  $N_t$ , or if the input number of RX antenna elements per row  $W_r$  is larger than the input number of RX antenna elements  $N_r$ , or if  $W_t(W_r)$  does not divide  $N_t(N_r)$ , or if the input distance within foliage is larger than the lower bound of the T-R separation distance, or if the TX/RX azimuth/elevation HPBW exceeds the predefined range, a corresponding error message will pop up. Users shall click “OK” on the error bar, then click the dark green button “Reset” to reset the input parameters, and the following steps are identical to those described above.

## 2.2 Output Files

### 2.2.1 Output Figures

For each simulation run, five figures will be generated and stored that are based on the particular results of the simulation that is being run, and an additional figure of path loss scatter plot will be generated and stored after  $N$  ( $N \geq 1$ ) continuous simulation runs with the same input parameters are complete. Note that the T-R separation distance is not an input parameter, but, instead, the lower bound and upper bound of the T-R separation distance are input parameters, such that the actual T-R separation distance will vary automatically among different simulation runs. Regardless of the number of simulation runs (RX locations), the five figures generated from the first simulation run, as well as the last figure generated for  $N$  ( $N \geq 1$ ) continuous simulation runs with the same input parameters, will pop up on the screen for visual purposes. The contents of those figures are as follows:

- Three-dimensional (3D) angle of departure (AOD) power spectrum, as illustrated in Fig. 2.2.
- 3D angle of arrival (AOA) power spectrum, as shown in Fig. 2.3.
- A sample omnidirectional power delay profile (PDP), as displayed in Fig. 2.4. Some fundamental information such as the frequency, environment, T-R separation distance, RMS delay spread, omnidirectional received power, omnidirectional path loss, and path loss exponent (PLE) [1], [2] is displayed on the PDP plot. The red solid line on the PDP denotes the noise threshold (i.e., the minimum received power of each resolvable multipath component) determined by the transmit power, dynamic range of our measurement system (180 dB), and a 10 dB SNR, i.e., the threshold equals the transmit power in logarithmic scale minus 170 dB.
- A sample directional PDP with strongest power, where directional antenna gain patterns are implemented at the TX and/or RX, as depicted in Fig. 2.5. This figure is generated by allowing users to implement arbitrary directional antenna patterns (gains and HPBWs) in an omnidirectional PDP, since directional antennas/antenna arrays will be utilized at the TX and/or the RX in a realistic mmWave communication system to provide gains to compensate for the higher free space path loss at mmWave frequencies. To obtain the directional PDP with

the strongest received power, NYUSIM searches for the best pointing angle out of all possible pointing angles, using the specified antenna details (i.e., azimuth and elevation HPBWs of TX and RX antennas) after first generating the omnidirectional PDP, such that the pointing angle of the TX and RX are found that gives the strongest received power. The TX/RX antenna gain pattern is calculated by NYUSIM using Eq. (2.1) in this user manual by employing the azimuth and elevation HPBWs of TX and RX antennas specified by the user on the GUI. This feature makes the channel simulator more valuable as it shows how a PDP will look like in a channel with directional antennas/antenna arrays used at the communication link end. On the directional PDP figure, relevant channel and antenna parameters, such as the frequency, environment, T-R separation distance, directional RMS delay spread, directional received power, directional path loss, directional PLE, and TX and RX antenna HPBWs and gains, are also displayed, where the directional path loss equals the transmit power plus TX and RX antenna gains, minus the directional received power [2], [6], [7].

- A series of PDPs over each receive antenna element obtained using Eq. (3) of [19], as shown in Fig. 2.6, where the antenna array type, number of antenna elements, and antenna element spacing are specified on the GUI by the user.
- A path loss scatter plot entitled "PathLossPlot" generated after  $N$  ( $N \geq 1$ ) continuous simulation runs with the same input parameters, as illustrated in Fig. 2.7. This figure shows omnidirectional path loss and directional path loss values for over the entire distance range generated from the  $N$  ( $N \geq 1$ ) continuous simulation runs, along with the fitted PLE and shadow fading standard deviation using the minimum-mean-square-error (MMSE) method [5], [7]. In the legend of the figure "PathLossPlot",  $n$  denotes the path loss exponent (PLE),  $\sigma$  is the shadow fading standard deviation, "omni" denotes omnidirectional, "dir" represents directional, and "dir-best" means the direction with the strongest received power. For producing the directional path loss at each RX location, NYUSIM searches for all possible pointing angles in increments of the azimuth and elevation HPBWs of the TX/RX antenna specified by the user on the GUI after first generating the omnidirectional PDP. The TX/RX antenna gain pattern is calculated by NYUSIM using Eq. (2.1) in this user manual based on the azimuth and elevation HPBWs of TX and RX antennas specified by the user on the GUI. The directional path loss is equal to the transmit power plus the TX and RX antenna gains, minus the directional received power [1], [2], [20], [21]. For generating Fig. 2.7, the antenna azimuth and elevation HPBWs are set to  $10.9^\circ$  and  $8.6^\circ$ , respectively, at both the TX and the RX, to match the antenna HPBWs used in the 28 GHz measurements [1], [2]. The simulated PLE and shadow fading standard deviation values agree well with the measured results presented in Table V and Table VIII of [2]. Directional path loss and directional PLE will always be larger (i.e., a directional channel is more lossy) than the omnidirectional case, because the directional antenna

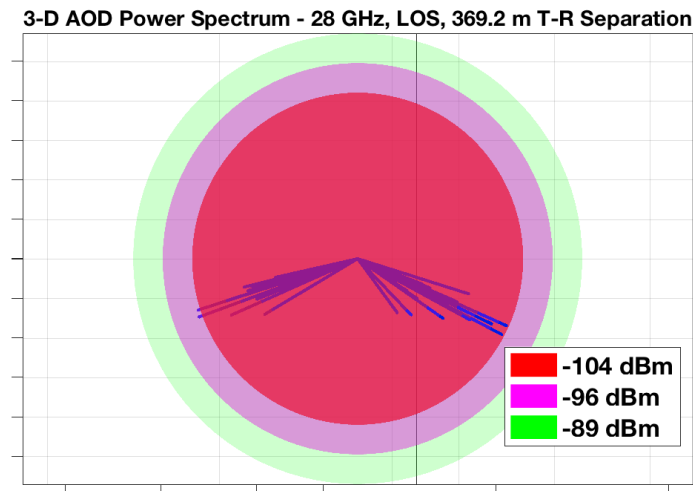


FIGURE 2.2: Example of a 3D AOD power spectrum generated from NYUSIM.

will spatially filter out many multipath components due to its directional pattern, such that the RX receives fewer multipath components hence less energy, thereby the directional path loss is higher after removing the antenna gain effect from the received power [2], [7].

### 2.2.2 Output Data Files

For each simulation run, five sets of .txt files and five corresponding .mat files are generated, namely, "AODLobePowerSpectrum $n$ \_Lobe $x$ .txt", "AODLobePowerSpectrum $n$ .mat", "AOALobePowerSpectrum $n$ \_Lobe $x$ .txt", "AOALobePowerSpectrum $n$ .mat", "OmniPDP $n$ .txt", "OmniPDP $n$ .mat", "DirectionalPDP $n$ .txt", "DirectionalPDP $n$ .mat", "SmallScalePDP $n$ .txt", and "SmallScalePDP $n$ .mat", where  $n$  denotes the  $n^{\text{th}}$  RX location (i.e.,  $n^{\text{th}}$  simulation run), and  $x$  represents the  $x^{\text{th}}$  spatial lobe. After  $N$  ( $N \geq 1$ ) continuous simulation runs with the same input parameters are complete, another three .txt files and three corresponding .mat files are produced, i.e., "BasicParameters.txt", "BasicParameters.mat", "OmniPDPInfo.txt", "OmniPDPInfo.mat", "DirPDPInfo.txt", and "DirPDPInfo.mat".

Each text file "AODLobePowerSpectrum $n$ \_Lobe $x$ " is associated with the output figure of 3D AOD power spectrum, and contains five parameters (columns) of each resolvable multipath component in an AOD spatial lobe, which are listed and explained below.

1. pathDelay (ns): an array containing the absolute propagation time delays of all resolvable multipath components in nanoseconds (ns).
2. pathPower (mWatts): an array containing the received powers of all resolvable multipath components in mWatts.

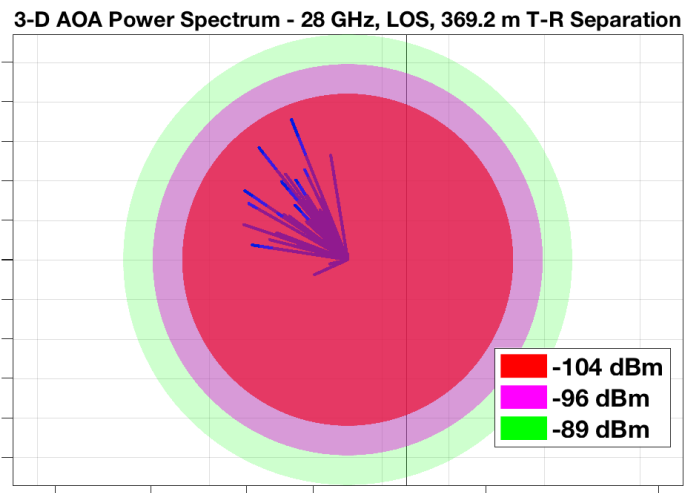


FIGURE 2.3: Example of a 3D AOA power spectrum generated from NYUSIM.

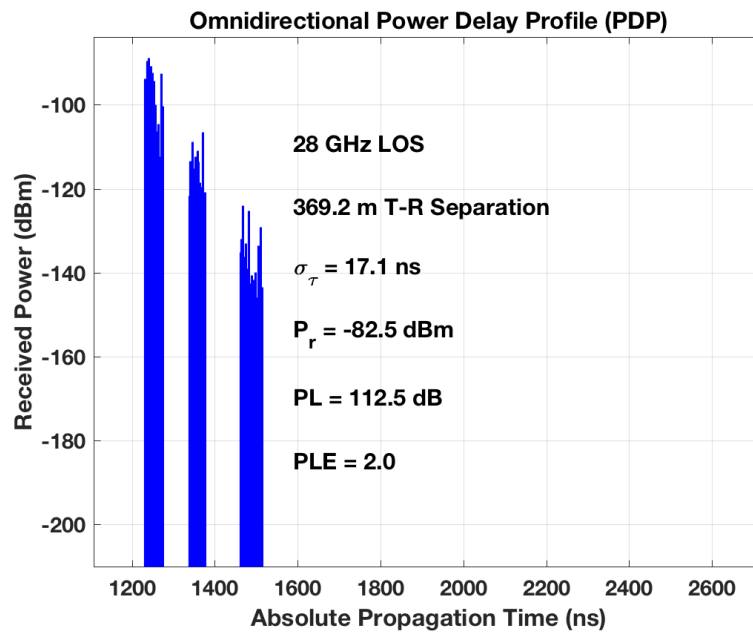


FIGURE 2.4: Example of an omnidirectional PDP generated from NYUSIM.

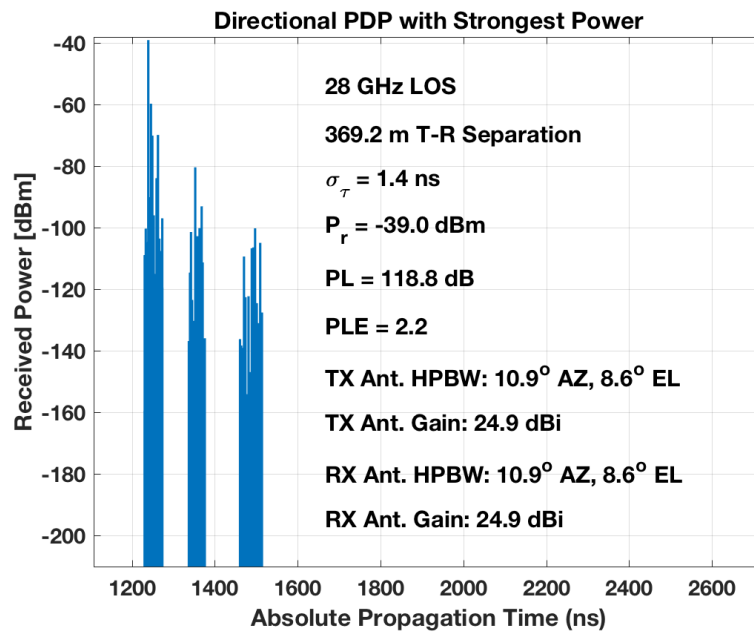


FIGURE 2.5: Example of an directional PDP with the strongest received power generated from NYUSIM. "Ant." denotes antenna.

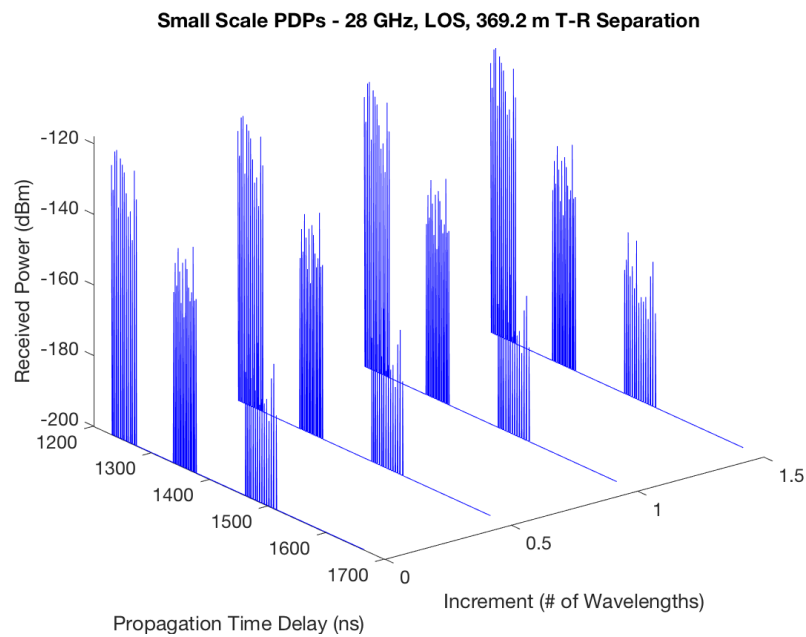


FIGURE 2.6: Example of the PDPs over different receive antenna elements generated from NYUSIM.

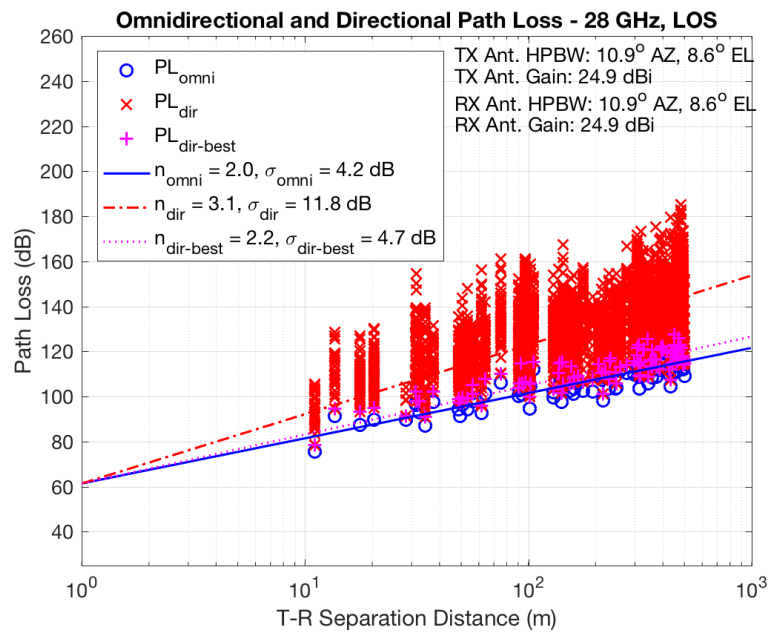


FIGURE 2.7: Example of a scatter plot showing the omnidirectional and directional path loss values generated from NYUSIM with 100 simulation runs for the 28 GHz UMi LOS scenario.  $n$  denotes the pass loss exponent (PLE),  $\sigma$  is the shadow fading standard deviation, "omni" denotes omnidirectional, "dir" represents directional, "dir-best" means the direction with the strongest received power, "Ant." denotes antenna, "AZ" and "EL" stand for azimuth and elevation, respectively.

3. pathPhase (rad): an array containing the phases of all resolvable multipath components in radians.
4. AOD (degree): an array containing the azimuth AODs of all resolvable multipath components in degrees.
5. ZOD (degree): an array containing the ZODs of all resolvable multipath components in degrees.

Note that inside the corresponding .mat file “AODLobePowerSpectrum $n$ ” is a structure containing the lobe matrices, each of which is composed of five columns as described above.

Each text file “AOALobePowerSpectrum $n$ \_Lobe $x$ ” is associated with the output figure of 3D AOA power spectrum, and contains five parameters (columns) of each resolvable multipath component in an AOA spatial lobe, which are listed and explained below.

1. pathDelay (ns): an array containing the absolute propagation time delays of all resolvable multipath components in nanoseconds (ns).
2. pathPower (mWatts): an array containing the received powers of all resolvable multipath components in mWatts.
3. pathPhase (rad): an array containing the phases of all resolvable multipath components in radians.
4. AOA (degree): an array containing the azimuth AOAs of all resolvable multipath components in degrees.
5. ZOA (degree): an array containing the ZOAs of all resolvable multipath components in degrees.

Note that inside the corresponding .mat file “AOALobePowerSpectrum $n$ ” is a structure containing the lobe matrices, each of which is composed of five columns as described above.

Each .txt and .mat file “OmniPDP $n$ ” is associated with the output figure of omnidirectional PDP, and contains two columns: the first column denotes the propagation time delay in nanoseconds, and the second column represents the received power in dBm.

Each .txt and .mat file “DirectionalPDP $n$ ” is associated with the output figure of omnidirectional PDP with directional antenna gain patterns implemented, and contains two columns: the first column denotes the propagation time delay in nanoseconds, and the second column represents the received power in dBm.

Each .txt and .mat file “SmallScalePDP $n$ ” is associated with the output figure of the series of omnidirectional PDPs over RX antenna elements, and contains three columns: the first column denotes the receiver antenna separation in terms of number of wavelengths, the second column is the propagation time delay in nanoseconds, and the third column represents the received power in dBm. Note that the noise power is set to -150 dBm for

visual purpose.

The text file "BasicParameters.txt" and the .mat file "BasicParameters.mat" subsume all the input parameter values as shown on the GUI when running the simulation.

The text file "OmniPDPInfo.txt" and the .mat file "OmniPDPInfo.mat" contain four columns where each column represents a key parameter for each of the  $N$  omnidirectional PDPs from  $N$  continuous simulation runs. The parameters are listed and explained below.

1. T-R Separation Distance (m)
2. Received Power (dBm): omnidirectional received power in dBm
3. Path Loss (dB): omnidirectional path loss in dB
4. RMS Delay Spread (ns): omnidirectional RMS delay spread in nanosecond (ns)

The text file "DirPDPInfo.txt" and the .mat file "DirPDPInfo.mat" contain 11 columns where each column represents a key parameter for each of the directional PDPs from  $N$  continuous simulation runs, where the same kind of parameters from each simulation run are cascaded in the same column. The parameters are listed and explained below.

1. Simulation run number
2. T-R Separation Distance (m)
3. Time Delay (ns): absolute propagation time delay of each resolvable multipath component in ns
4. Received Power (dBm): received power of each resolvable multipath component in dBm without antenna gains
5. Phase (rad): phase of each resolvable multipath component in radians
6. Azimuth AoD (degree): azimuth AoD of each resolvable multipath component in degrees
7. Elevation AoD (degree): elevation AoD of each resolvable multipath component in degrees
8. Azimuth AoA (degree): azimuth AoA of each resolvable multipath component in degrees
9. Elevation AoA (degree): elevation AoA of each resolvable multipath component in degrees
10. Path Loss (dB): directional path loss obtained by aligning the TX/RX antenna boresight on the AoD/AoA of each resolvable multipath component. The directional path loss equal the transmit power plus the TX/RX antenna boresight gains, minus directional received power.
11. RMS Delay Spread (ns): directional RMS delay spread in ns for each directional PDP

### 3. Channel Model Supported by NYUSIM

The broadband statistical spatial channel model (SSCM) [3] developed by NYU is used in NYUSIM.

#### 3.1 Path Loss Model

The close-in free space reference distance (CI) path loss model with a 1 m anchor point, with an extra attenuation term due to various atmospheric attenuation factors [13], is employed in NYUSIM, which is expressed as [2], [5], [22]:

$$\text{PL}^{\text{CI}}(f, d)[\text{dB}] = \text{FSPL}(f, 1 \text{ m})[\text{dB}] + 10n\log_{10}(d) + \text{AT}[\text{dB}] + \chi_{\sigma}^{\text{CI}}, \quad (3.1)$$

where  $d \geq 1 \text{ m}$

where  $f$  denotes the carrier frequency in GHz,  $d$  is the 3D T-R separation distance,  $n$  represents the path loss exponent (PLE), AT is the attenuation term induced by the atmosphere,  $\chi_{\sigma}^{\text{CI}}$  is a zero-mean Gaussian random variable with a standard deviation  $\sigma$  in dB, and  $\text{FSPL}(f, 1 \text{ m})$  denotes the free space path loss in dB at a T-R separation distance of 1 m at the carrier frequency  $f$ :

$$\text{FSPL}(f, 1 \text{ m})[\text{dB}] = 20\log_{10}\left(\frac{4\pi f \times 10^9}{c}\right) = 32.4[\text{dB}] + 20\log_{10}(f) \quad (3.2)$$

where  $c$  is the speed of light, and  $f$  is in GHz. The term AT is characterized by:

$$\text{AT}[\text{dB}] = \alpha[\text{dB/m}] \times d[\text{m}] \quad (3.3)$$

where  $\alpha$  is the attenuation factor in dB/m for the frequency range of 1 GHz to 100 GHz, which includes the collective attenuation effects of dry air (including oxygen), water vapor, rain, and haze [13].  $d$  is the 3D T-R separation distance as in (3.1).

Fig. 3.1 illustrates example propagation attenuation values due to dry air, vapor, haze, and rain at mmWave frequencies from 1 GHz to 100 GHz, with a barometric pressure of 1013.25 mbar, a relative humidity of 80%, a temperature of 20°C, and a rain rate of 5 mm/hr, while the collective attenuation effects of these four main natural absorbers are displayed in Fig. 3.2. These results were obtained and reproduced from five reported controlled experiments on atmospheric attenuation [13].

Note that the CI model inherently has an intrinsic frequency dependency of path loss already embedded within the FSPL term. A useful property

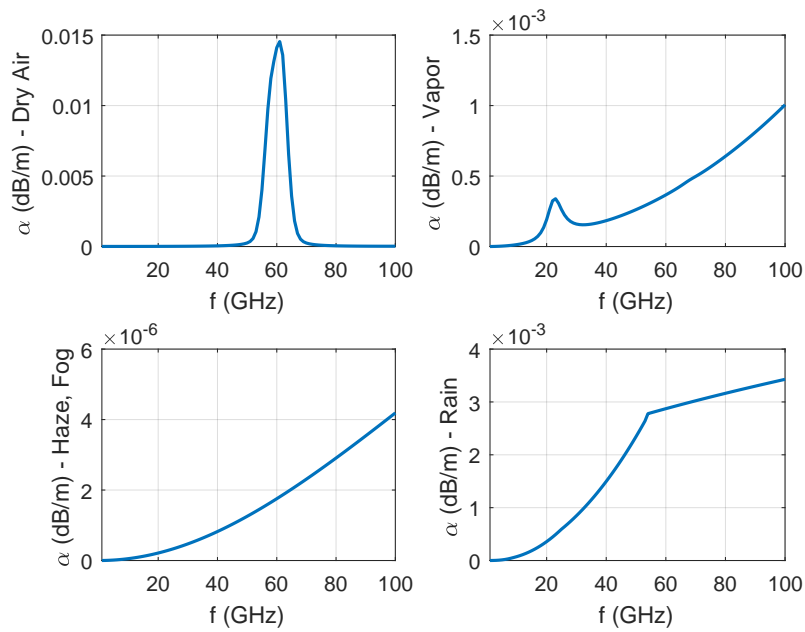


FIGURE 3.1: Propagation attenuation due to dry air, vapor, haze, and rain at mmWave frequencies, with a barometric pressure of 1013.25 mbar, a relative humidity of 80%, a temperature of 20°C, and a rain rate of 5 mm/hr [13].

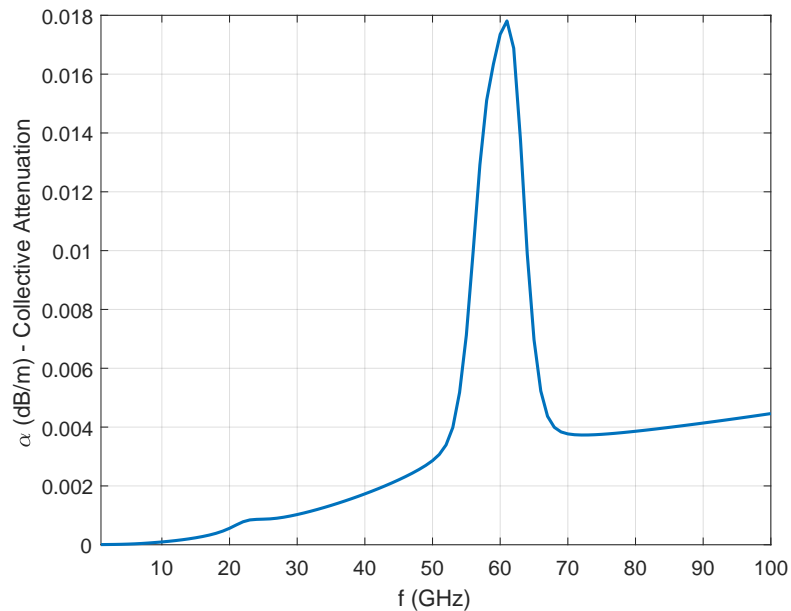


FIGURE 3.2: Collective attenuation effects of dry air, vapor, haze, and rain at mmWave frequencies, with a barometric pressure of 1013.25 mbar, a relative humidity of 80%, a temperature of 20°C, and a rain rate of 5 mm/hr [13].

of (3.1) is that  $10n$  describes path loss in dB in terms of decades of distances beginning at 1 m (making it very easy to compute power over distance in one's mind).

The CI path loss model is based on fundamental principles of wireless propagation, dating back to Friis and Bullington, where the PLE parameter offers insight into path loss based on the environment, having a PLE value of 2 in free space (as shown by Friis) and a value of 4 for the asymptotic two-ray ground bounce propagation model (as shown by Bullington). Standardizing to a reference distance of 1 m makes comparisons of measurements and models simple, and provides a standard definition for the PLE, while enabling intuition and rapid computation of path loss [5].

Compared with the existing alpha-beta-gamma (ABG) path loss model used in 3GPP/ITU channel models [5], [7], [12], the CI model has an identical mathematical form, while offering intuitive appeal, better model parameter stability, and better prediction performance over a vast range of microwave and mmWave frequencies, distances, and scenarios, with fewer parameters [5].

In the current version of NYUSIM, the PLE  $n$  is set to the free space PLE of 2 with a shadow fading standard deviation of 4.0 dB for the LOS environment, while the PLE and shadow fading standard deviation are respectively set to 3.2 and 7.0 dB for the NLOS environment [2], [3], for both UMi and UMa scenarios. For the RMa scenario, the LOS PLE and shadow fading standard deviation are 2.16 and 4.0 dB, respectively, while the NLOS PLE and shadow fading standard deviation are 2.75 and 8.0 dB, respectively (please refer to [8], [9] for more information). Note that although the channel parameters for the UMi scenario are also used for the UMa and RMa (except for the path loss model parameters) scenarios in this simulator, users can adjust the UMa and RMa channel parameters in the source code according to their own needs.

## 3.2 Wideband Temporal/Spatial Clustering Algorithm

The SSCM given here utilizes *time clusters* (TC) and *spatial lobes* (SL) to model the omnidirectional CIR and corresponding joint AOD/AOA power spectra, which have been used successfully in modeling mmWave channels [3]. *Time clusters* are composed of multipath components traveling close in time, and that arrive from potentially different angular directions in a short propagation time window. *Spatial lobes* represent main directions of arrival (or departure) where energy arrives over several hundred nanoseconds. This SSCM structure is motivated by field measurements, which have shown that multiple paths within a time cluster can arrive at unique pointing angles, detectable due to high gain directional antennas, and this feature has not been modeled in current 3GPP and WINNER models. These definitions de-couple the time and space dimensions by extracting temporal and spatial statistics separately. The definition of time cluster here considers multipath components traveling close in time, but that can arrive from

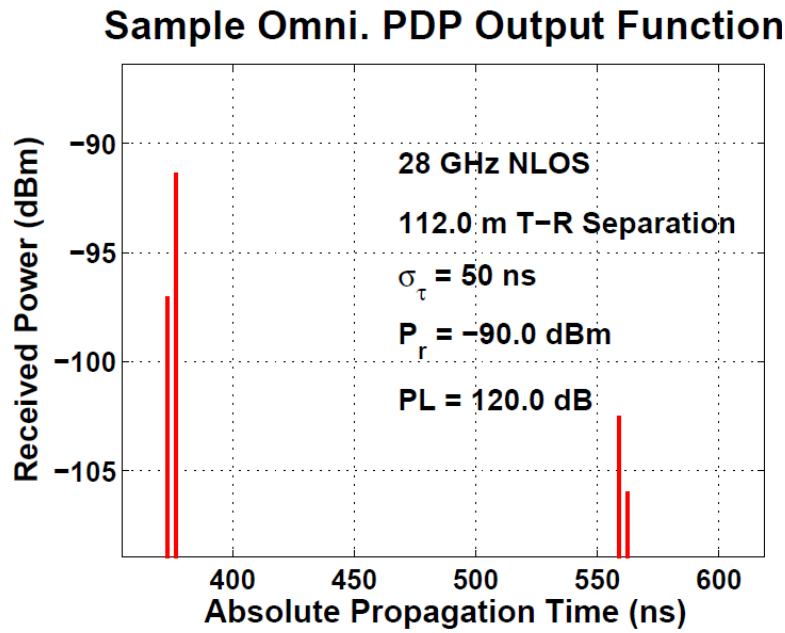


FIGURE 3.3: Example of an omnidirectional PDP with four multipath taps [3].

many angular directions, whereas current 3GPP and WINNER models assume that subpaths belonging to a cluster travel along the same propagation path, but arrive at the same time delay over a certain AOA angular spread.

The TCSL approach implements a physically-based clustering scheme (e.g., the use of a fixed inter-cluster void interval representing the minimum propagation time between likely reflection or scattering objects) derived from field observations, and can be used to extract time cluster and spatial lobe statistics for any ray-tracing or measurement data sets [3]. The time-partitioning methodology delineates the beginning and end times of each time cluster, using a 25 ns minimum inter-cluster void interval. Sequentially arriving multipath components that occur within 25 ns of each other are assumed to belong to one time cluster. The 3D spatial distribution of received power was reconstructed from the 28 GHz and 73 GHz LOS and NLOS directional received powers by linearly interpolating adjacent power level segments in azimuth and elevation with a  $1^\circ$  resolution, and extracting 3D spatial angular statistics. A -10 dB threshold below maximum peak power in the 3D power spectrum is used in both LOS and NLOS environments, where all power segments below this threshold are disregarded for further processing. Fig. 3.3 illustrates an omnidirectional PDP, where there are four multipath taps which are grouped into two time clusters with exponentially decaying amplitudes. The four multipath taps are then grouped into two AOA spatial lobes, as shown in Fig. 3.4.

### 3-D AOA Power Spectrum - 28 GHz NLOS

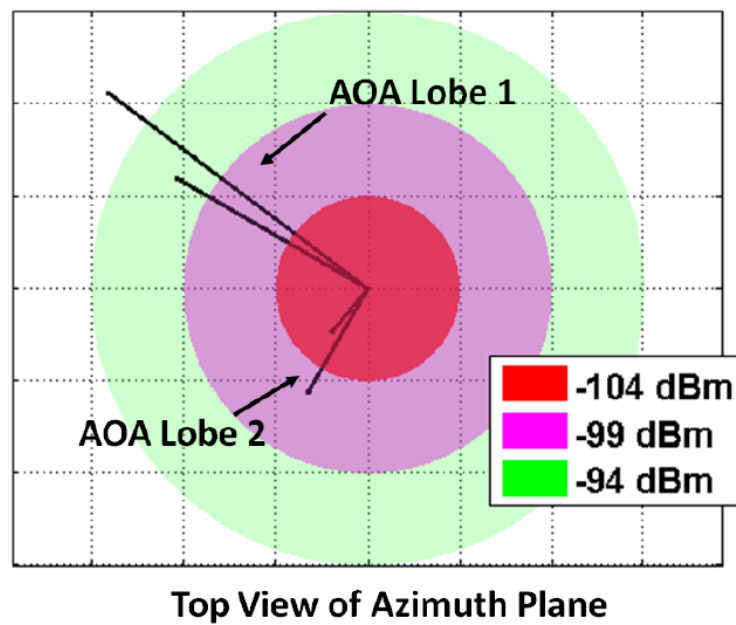


FIGURE 3.4: Example of an AOA power spectrum with four multipath taps [3].

## 4. Applications of NYUSIM

The output figure and data files generated from NYUSIM can be used in various ways based on users' needs, e.g., to simulate channel impulse responses for mmWave systems, to investigate MIMO performance, etc.

### 4.1 MIMO Channel Condition Number

First we show an example of how to obtain the condition number of a MIMO channel by making use of the output data files "BasicParameters.mat" and "DirPDPInfo.mat", assuming OFDM modulation is utilized.

The condition number is defined as the ratio of the largest to smallest singular value in the singular value decomposition of a matrix, and is a metric to characterize the quality of MIMO channels in the context of wireless communications [22]–[25]. The condition number will be high (e.g., over 20 dB) if the minimum singular value is close to zero, and will be 0 dB if singular values are equal. Physically, a small condition number value (e.g., below 20 dB) indicates good orthogonality of different sub-channels (a sub-channel usually has a distinct spatial direction), and the channel gains are comparable in different spatial directions. The rank of a matrix is the dimension of the vector space generated (or spanned) by its columns (or rows) [26], and it determines how many data streams can be multiplexed over the channel in the context of MIMO communications [23], [27], [28]. The condition number is related to the rank of a matrix: a low condition number usually corresponds to a high rank and vice versa; the matrix has full rank (the highest rank) when the condition number is equal or close to 0 dB (the lowest theoretical condition number).

Let's look at the condition number of a MIMO channel matrix for a single sub-carrier in an OFDM system. As described in Section 2.2.2, the output data files "BasicParameters.mat" and "DirPDPInfo.mat" contain paramount parameters of each resolvable multipath component, which will be useful in generating the MIMO channel coefficient for an OFDM sub-carrier. Take ULAs at both the transmitter and receiver for example, the equation for generating such a channel coefficient is provided below, which is adapted from Eq.(2) in [29]:

$$h_{m,k}(f) = \sum_p \alpha_{m,k,p} e^{j\Phi_{m,k,p}} e^{-j2\pi f \tau_{m,k,p}} e^{-j2\pi d_T m \sin(\phi_{m,k,p})} e^{-j2\pi d_R k \sin(\varphi_{m,k,p})} \quad (4.1)$$

where  $h_{m,k}(f)$  denotes the MIMO channel coefficient between the  $m^{th}$  transmit antenna and the  $k^{th}$  receive antenna for the sub-carrier  $f$ ,  $p$  represents

the  $p^{th}$  resolvable multipath component,  $\alpha$  is the amplitude of the channel gain,  $\Phi$  denotes the phase of the multipath component,  $\tau$  represents the time delay,  $d_T$  and  $d_R$  are the antenna element spacing at the transmitter and receiver, respectively, while  $\phi$  and  $\varphi$  denote the azimuth angle of departure and angle of arrival, respectively. All of the above parameters can be extracted from the files "BasicParameters.mat" and "DirPDPInfo.mat". For each sub-carrier  $f$  in a MIMO-OFDM system, there exists an  $N_t \times N_r$  channel matrix  $H$  whose elements are  $h_{m,k}(f)$ , where  $m = 1, \dots, N_t$  and  $k = 1, \dots, N_r$ . The condition number of  $H$  can be obtained consequently.

Using the above mentioned approach, and the input parameters on the NYUSIM GUI with the following values:

- Frequency: 28 GHz
- RF bandwidth: 800 MHz
- Scenario: UMi
- Environment: LOS
- Lower Bound of T-R Separation Distance: 100 m
- Upper Bound of T-R Separation Distance: 100 m
- TX Power: 30 dBm
- Number of RX Locations: 100
- Barometric Pressure: 1013.25 mbar
- Humidity: 50%
- Temperature: 20°C
- Rain Rate: 0 mm/hr
- Polarization: Co-Pol
- Foliage Loss: No
- TX Array Type: ULA
- RX Array Type: ULA
- Number of TX Antenna Elements  $N_t$ : 2
- Number of RX Antenna Elements  $N_r$ : 2
- TX Antenna Spacing: 0.5 wavelength
- RX Antenna Spacing: 0.5 wavelength
- Number of TX Antenna Elements Per Row  $W_t$ : 2
- Number of RX Antenna Elements Per Row  $W_r$ : 2
- TX Antenna Azimuth HPBW: 10°

- TX Antenna Elevation HPBW:  $10^\circ$
- RX Antenna Azimuth HPBW:  $10^\circ$
- RX Antenna Elevation HPBW:  $10^\circ$

and assuming the frequency interval between adjacent sub-carriers is 500 kHz, which corresponds to  $800 \text{ MHz}/500 \text{ kHz} = 1600$  sub-carriers, we perform 100 simulation runs (i.e., set the number of RX locations to 100) to emulate 100 random MIMO channel realizations with the input parameters described above. Then the following changes are made to the four input parameters below with all the other input parameter values remaining the same:

- Number of TX Antenna Elements  $N_t$ : 3
- Number of RX Antenna Elements  $N_r$ : 3
- Number of TX Antenna Elements Per Row  $W_t$ : 3
- Number of RX Antenna Elements Per Row  $W_r$ : 3

Fig. 4.1 illustrates the empirical CDF of the condition number of channel matrices for OFDM sub-carriers with the above two sets of input parameters in one of the 100 simulation runs. The empirical CDF of the corresponding rank of the channel matrices are plotted in Fig. 4.2, where the rank here is defined as the number of singular values of the channel matrix that are larger than  $\sigma_m/1000$ , where  $\sigma_m$  is the maximum singular value of the channel matrix. By this definition of rank, we are essentially ignoring the singular values that are 30 dB smaller than the maximum singular value, which is physically reasonable since the singular value is a measure of the channel gain along its corresponding singular vector and it makes little sense to consider the direction with an extremely small channel gain. It is apparent from Fig. 4.1 that the condition numbers of the individual OFDM sub-carriers for a  $3 \times 3$  MIMO channel is about 18 dB larger compared to the  $2 \times 2$  case on average, and the relatively large condition number of the  $3 \times 3$  channel matrix may stem from the fact that the matrix is rank deficient, as evident from Fig. 4.2, in which about 96% of the channel matrices have a rank of 2 instead of 3 (full rank).

Based on the results from the 100 random simulation runs, it is found that the average median value of the condition numbers of the channel matrices for individual sub-carriers over the 100 simulation runs is around 13 dB (i.e., the difference in dB between the largest and smallest singular value of the channel matrix is 13 dB), and the average matrix rank is 2. When the numbers of TX and RX antenna elements are both changed to 3, the average median value of the condition number increase to 31 dB, with a mean rank of roughly 2, indicating that two spatial streams can be sent simultaneously using the spatial multiplexing technique in this case.

The Matlab code for extracting channel coefficients based on Eq. (4.1), generating the channel matrix for each sub-carrier frequency, and calculating the condition number and rank in the example above is contained in the package named "Application Example Code" available on the NYUSIM

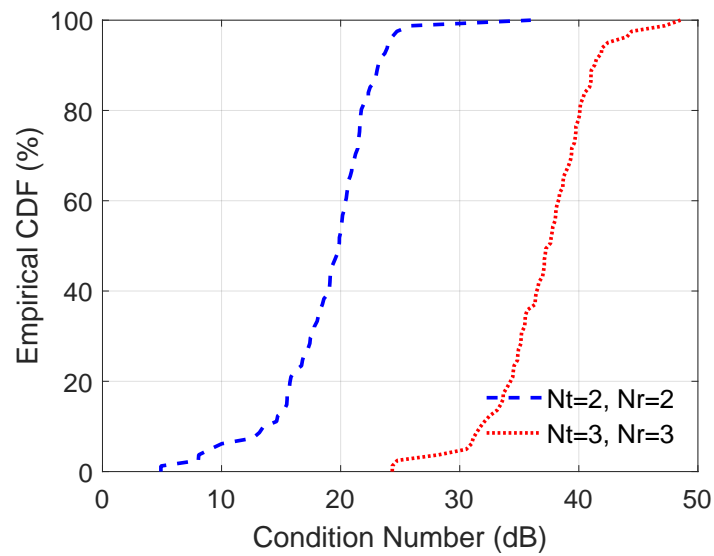


FIGURE 4.1: Empirical CDF of the condition number of channel matrices for OFDM sub-carriers with different transmit and receive antenna elements  $N_t$  and  $N_r$  for MIMO-OFDM channels in one simulation run.

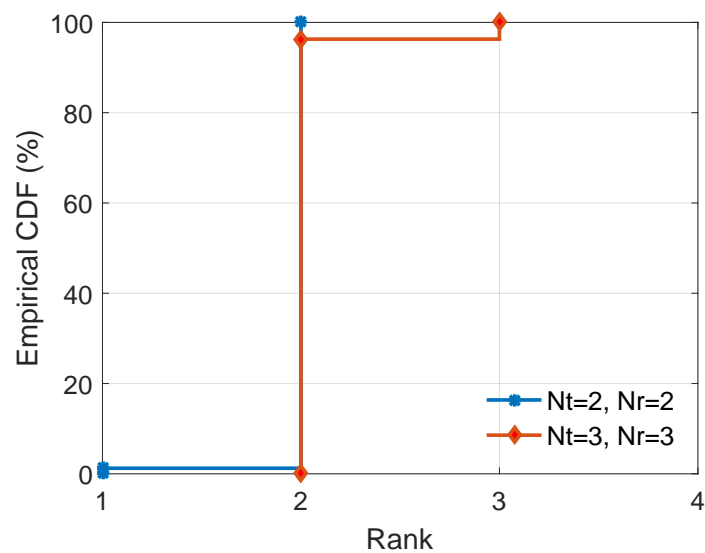


FIGURE 4.2: Empirical CDF of the rank of channel matrices for OFDM sub-carriers with different transmit and receive antenna elements  $N_t$  and  $N_r$  for MIMO-OFDM channels in one simulation run.

downloading website.

## 4.2 Spectral Efficiency Comparison Between 3GPP and NYUSIM Channel Models

As mentioned in NYUSIM Overview on Page ii of this user manual, the 3GPP TR 38.900 Release 14 channel model [12] contains unrealistic number of clusters (e.g., 19 clusters for UMi NLOS) and up to 20 rays per cluster, which is excessively large and not borne out by measurements, and is likely to result in incorrect predictions on MIMO system performance such as spectral efficiency (SE). In this subsection, we use the 3GPP TR 38.900 Release 14 channel model [12] and NYUSIM channel model to analyze and compare the spectral efficiency for mmWave MIMO channels.

Let us assume a single-cell single-user MIMO system without multiple-access interference, operating at 28 GHz with an RF bandwidth of 100 MHz in the UMi scenario. The base station (BS) is equipped with 256 antenna elements comprising a uniform rectangular array (URA) with cross-polarized elements, which can reduce the hardware size and make better use of multipath components with different polarizations since the cross-polarization discrimination ratio is 8-9 dB in both models, where the antenna pattern on Page 23 of [12] is adopted. The user equipment (UE) has 16 antenna elements constituting a URA with cross-polarized omnidirectional elements. Signal-to-noise ratios (SNRs) are fixed at certain values to investigate the SE achieved by the 3GPP [12] and NYUSIM models described in [3] and Section 3 of this user manual. Two hundred random channel realizations using random distances ranging from 10 to 435 m were performed for each channel model, where the NYUSIM code runs about 30 times faster than the 3GPP code.

Fig. 4.3 illustrates the SE achieved by the hybrid beamforming algorithm proposed in [30] for a  $256 \times 16$  mmWave system at 28 GHz with rectangular planar arrays at the transmitter and receiver for various numbers of data streams  $N_s$ , using the 3GPP and NYUSIM models. As shown by Fig. 4.3, the SE generated by the 3GPP channel model is just slightly smaller than that yielded by the NYUSIM channel model for  $N_s = 1$ , but much larger for  $N_s = 4$ . For instance, for an SNR of 20 dB and  $N_s = 4$ , the 3GPP SE (40 bits/s/Hz) is about 13 bits/s/Hz greater than the NYUSIM SE (about 27 bits/s/Hz). This is likely because NYUSIM yields one or two strong dominant clusters and much weaker non-dominant clusters, while the 3GPP model has less focused directional energy than what realistically exists. The results indicate that the 3GPP channel model is optimistic when predicting diversity and the achievable SE at mmWave frequencies, while NYUSIM provides realistic channel parameters and SE predictions due to the use of extensive real-world measurement data at mmWave frequencies, thus could help avoid system errors inherent with legacy modeling approaches.

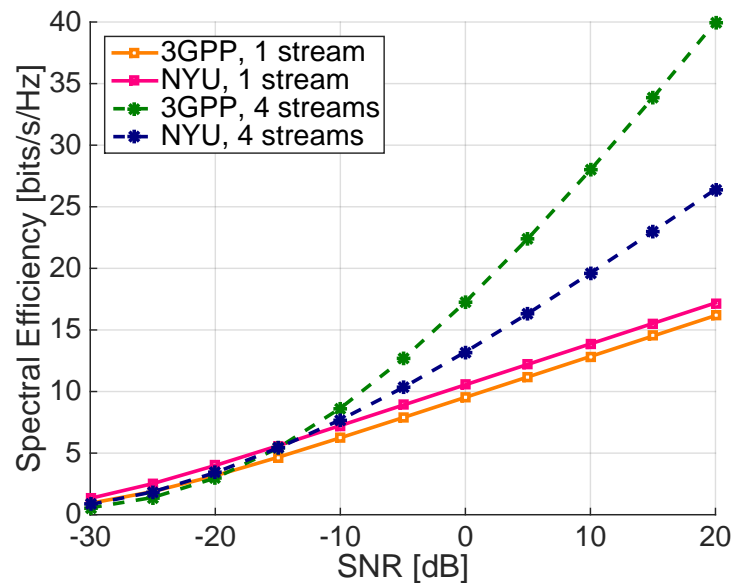


FIGURE 4.3: Spectral efficiency achieved by hybrid beamforming for a  $256 \times 16$  system at 28 GHz with rectangular antenna arrays at the transmitter and receiver with four RF chains.

Apart from the example demonstrated above, NYUSIM can also find applications in other types of analysis, such as the design of antenna arrays [31] and bit error simulation [10], [32].

## Bibliography

- [1] T. S. Rappaport, S. Sun, R. Mayzus, H. Zhao, Y. Azar, K. Wang, G. N. Wong, J. K. Schulz, M. Samimi, and F. Gutierrez, "Millimeter wave mobile communications for 5G cellular: It will work!", *IEEE Access*, vol. 1, pp. 335–349, 2013. [Online]. Available: <http://ieeexplore.ieee.org/document/6515173/>.
- [2] T. S. Rappaport, G. R. MacCartney, Jr., M. K. Samimi, and S. Sun, "Wideband millimeter-wave propagation measurements and channel models for future wireless communication system design (*Invited Paper*)", *IEEE Transactions on Communications*, vol. 63, no. 9, pp. 3029–3056, 2015. [Online]. Available: <http://ieeexplore.ieee.org/document/7109864/>.
- [3] M. K. Samimi and T. S. Rappaport, "3-D millimeter-wave statistical channel model for 5G wireless system design", *IEEE Transactions on Microwave Theory and Techniques*, vol. 64, no. 7, pp. 2207–2225, 2016. [Online]. Available: <http://ieeexplore.ieee.org/document/7501500/>.
- [4] —, "Local multipath model parameters for generating 5G millimeter-wave 3GPP-like channel impulse response", *the 10th European Conference on Antennas and Propagation (EuCAP 2016)*, 2016. [Online]. Available: <http://arxiv.org/abs/1511.06941>.
- [5] S. Sun *et al.*, "Investigation of prediction accuracy, sensitivity, and parameter stability of large-scale propagation path loss models for 5G wireless communications", *IEEE Transactions on Vehicular Technology*, vol. 65, no. 5, pp. 2843–2860, 2016. [Online]. Available: <http://ieeexplore.ieee.org/document/7434656/>.
- [6] S. Sun, G. R. MacCartney, M. K. Samimi, and T. S. Rappaport, "Synthesizing omnidirectional antenna patterns, received power and path loss from directional antennas for 5G millimeter-wave communications", in *2015 IEEE Global Communications Conference (GLOBECOM)*, 2015, pp. 1–7. [Online]. Available: <http://arxiv.org/abs/1511.07271>.
- [7] G. R. MacCartney, Jr., T. S. Rappaport, S. Sun, and S. Deng, "Indoor-office wideband millimeter-wave propagation measurements and channel models at 28 and 73 GHz for ultra-dense 5G wireless networks", *IEEE Access*, vol. 3, pp. 2388–2424, 2015. [Online]. Available: <http://ieeexplore.ieee.org/document/7289335/>.

- [8] G. R. MacCartney, Jr., S. Sun, T. S. Rappaport, Y. Xing, H. Yan, J. Koka, R. Wang, and D. Yu, "Millimeter wave wireless communications: New results for rural connectivity", in *All Things Cellular'16, in conjunction with ACM MobiCom*, 2016. [Online]. Available: <https://arxiv.org/abs/1608.05384>.
- [9] "Investigation of prediction accuracy, sensitivity, and parameter stability of large-scale propagation path loss models from 500 MHz to 100 GHz", [Online]. Available: [http://wireless.engineering.nyu.edu/presentations/NTIA-propagation-presentation-JUNE-15-2016\\_v1-3.pdf](http://wireless.engineering.nyu.edu/presentations/NTIA-propagation-presentation-JUNE-15-2016_v1-3.pdf).
- [10] V. Fung, T. S. Rappaport, and B. Thoma, "Bit error simulation for pi/4 DQPSK mobile radio communications using two-ray and measurement-based impulse response models", *IEEE Journal on Selected Areas in Communications*, vol. 11, no. 3, pp. 393–405, 1993. [Online]. Available: <http://ieeexplore.ieee.org/document/219546/>.
- [11] J. C. Liberti and T. S. Rappaport, "Analysis of CDMA cellular radio systems employing adaptive antennas in multipath environments", in *IEEE 46th Vehicular Technology Conference*, vol. 2, 1996, pp. 1076–1080. [Online]. Available: <http://ieeexplore.ieee.org/document/501477/>.
- [12] 3GPP, "Study on channel model for frequency spectrum above 6 GHz", 3rd Generation Partnership Project (3GPP), TR 38.900 V14.2.0, 2016. [Online]. Available: <http://www.3gpp.org/DynaReport/38900.htm>.
- [13] H. J. Liebe, G. A. Hufford, and M. G. Cotton, "Propagation modeling of moist air and suspended water/ice particles at frequencies below 1000 GHz", *AGARD Conference Proceedings 542*, 1993. [Online]. Available: <http://www.its.bldrdoc.gov/publications/2670.aspx>.
- [14] J. J. A. Lempinen, J. K. Laiho-Steffens, and A. F. Wacker, "Experimental results of cross polarization discrimination and signal correlation values for a polarization diversity scheme", in *IEEE 47th Vehicular Technology Conference*, vol. 3, 1997, pp. 1498–1502. [Online]. Available: <http://ieeexplore.ieee.org/document/605617/>.
- [15] H. lin Xiao, S. Ouyang, and Z. ping Nie, "The cross polarization discrimination of MIMO antennas at mobile station", in *International Conference on Communications, Circuits and Systems (ICCCAS)*, 2008, pp. 203–206. [Online]. Available: <http://ieeexplore.ieee.org/document/4657759/>.
- [16] T. S. Rappaport and S. Deng, "73 GHz wideband millimeter-wave foliage and ground reflection measurements and models", in *2015 IEEE International Conference on Communication Workshop (ICCW)*, 2015, pp. 1238–1243. [Online]. Available: <https://arxiv.org/pdf/1509.00436>.
- [17] T. S. Rappaport and R. A. Brickhouse, "A simulation of cellular system growth and its effect on urban in-building parasitic frequency reuse", *IEEE Transactions on Vehicular Technology*, vol. 48, no. 1, pp. 286–

- 294, 1999. [Online]. Available: <http://ieeexplore.ieee.org/document/740107/>.
- [18] T. Bai, A. Alkhateeb, and R. W. Heath, "Coverage and capacity of millimeter-wave cellular networks", *IEEE Communications Magazine*, vol. 52, no. 9, pp. 70–77, 2014. [Online]. Available: <http://ieeexplore.ieee.org/document/6894455/>.
- [19] A. Alkhateeb and R. W. Heath, "Frequency selective hybrid precoding for limited feedback millimeter wave systems", *IEEE Transactions on Communications*, vol. 64, no. 5, pp. 1801–1818, 2016. [Online]. Available: <http://ieeexplore.ieee.org/document/7448873/>.
- [20] A. I. Sulyman, A. T. Nassar, M. K. Samimi, G. R. Maccartney, T. S. Rappaport, and A. Alsanie, "Radio propagation path loss models for 5G cellular networks in the 28 GHz and 38 GHz millimeter-wave bands", *IEEE Communications Magazine*, vol. 52, no. 9, pp. 78–86, 2014. [Online]. Available: <http://ieeexplore.ieee.org/document/6894456/>.
- [21] A. I. Sulyman, A. Alwarafy, G. R. MacCartney, T. S. Rappaport, and A. Alsanie, "Directional radio propagation path loss models for millimeter-wave wireless networks in the 28-, 60-, and 73-GHz bands", *IEEE Transactions on Wireless Communications*, vol. 15, no. 10, pp. 6939–6947, 2016. [Online]. Available: <http://ieeexplore.ieee.org/document/7522613/>.
- [22] T. S. Rappaport, R. W. Heath, Jr., R. C. Daniels, and J. N. Murdock, *Millimeter Wave Wireless Communications*. Pearson/Prentice Hall 2015.
- [23] Q. H. Abbasi, H. E. Sallabi, E. Serpedin, K. Qaraqe, and A. Alomainy, "Condition number variability of ultra wideband MIMO on body channels", in *2016 International Workshop on Antenna Technology (iWAT)*, 2016, pp. 167–169. [Online]. Available: <http://ieeexplore.ieee.org/document/7434833/>.
- [24] R. W. Heath and D. J. Love, "Multimode antenna selection for spatial multiplexing systems with linear receivers", *IEEE Transactions on Signal Processing*, vol. 53, no. 8, pp. 3042–3056, 2005. [Online]. Available: <http://ieeexplore.ieee.org/document/1468498/>.
- [25] X. Lu, J. Wu, X. Huang, W. Li, J. Lu, and Z. Gong, "An improved semi-orthogonal user selection algorithm based on condition number for multiuser MIMO systems", *China Communications*, vol. 11, no. 13, pp. 23–30, 2014. [Online]. Available: <http://ieeexplore.ieee.org/document/7022522/>.
- [26] N. Bourbaki, *Elements of Mathematics, Algebra I*. Hermann 1974.
- [27] M. Matthaiou, D. I. Laurenson, and C. X. Wang, "Reduced complexity detection for rician MIMO channels based on condition number thresholding", in *2008 International Wireless Communications and Mobile Computing Conference*, 2008, pp. 988–993. [Online]. Available: <http://ieeexplore.ieee.org/document/4600070/>.

- [28] S. Sun, T. S. Rappaport, R. W. Heath, A. Nix, and S. Rangan, "MIMO for millimeter-wave wireless communications: Beamforming, spatial multiplexing, or both?", *IEEE Communications Magazine*, vol. 52, no. 12, pp. 110–121, 2014. [Online]. Available: <http://ieeexplore.ieee.org/document/6979962/>.
- [29] A. Adhikary, E. A. Safadi, M. K. Samimi, R. Wang, G. Caire, T. S. Rappaport, and A. F. Molisch, "Joint spatial division and multiplexing for mm-wave channels", *IEEE Journal on Selected Areas in Communications*, vol. 32, no. 6, pp. 1239–1255, 2014. [Online]. Available: <http://ieeexplore.ieee.org/document/6823686/>.
- [30] O. E. Ayach, S. Rajagopal, S. Abu-Surra, Z. Pi, and R. W. Heath, "Spatially sparse precoding in millimeter wave MIMO systems", *IEEE Transactions on Wireless Communications*, vol. 13, no. 3, pp. 1499–1513, 2014. [Online]. Available: <http://ieeexplore.ieee.org/document/6717211/>.
- [31] R. B. Ertel, P. Cardieri, K. W. Sowerby, T. S. Rappaport, and J. H. Reed, "Overview of spatial channel models for antenna array communication systems", *IEEE Personal Communications*, vol. 5, no. 1, pp. 10–22, 1998. [Online]. Available: <http://ieeexplore.ieee.org/document/656151/>.
- [32] B. Thoma, T. S. Rappaport, and M. D. Kietz, "Simulation of bit error performance and outage probability of pi/4 DQPSK in frequency-selective indoor radio channels using a measurement-based channel model", in *IEEE Global Telecommunications Conference (GLOBECOM)*, 1992, 1825–1829 vol.3. [Online]. Available: <http://ieeexplore.ieee.org/document/276698/>.